



Contents lists available at ScienceDirect

European Journal of Medicinal Chemistry

journal homepage: <http://www.elsevier.com/locate/ejmech>

Research paper

Discovery of novel PARP/PI3K dual inhibitors with high efficiency against BRCA-proficient triple negative breast cancer

Junwei Wang^{a,1}, Guangchao He^{b,1}, Hui Li^a, Yiran Ge^b, Shuping Wang^b, Yungen Xu^{a,b,**}, Qihua Zhu^{a,b,*}

^a State Key Laboratory of Natural Medicines, China Pharmaceutical University, Nanjing, 210009, China

^b Jiangsu Key Laboratory of Drug Design and Optimization, Department of Medicinal Chemistry, China Pharmaceutical University, Nanjing, 210009, China

ARTICLE INFO

Article history:

Received 20 September 2020

Received in revised form

17 November 2020

Accepted 24 November 2020

Available online xxx

Keywords:

Triple negative breast cancer

PARP/PI3K dual Inhibitors

Antitumor activity

Structural modifications

Structure-activity relationships

ABSTRACT

Co-targeting PARP and PI3K by PARP/PI3K dual inhibitors has been recognized as a promising chemotherapeutic strategy for the treatment of triple negative breast cancer (TNBC) in our previous work. To further explore novel and more potent PARP/PI3K dual inhibitors, a series of compounds were designed, synthesized and evaluated for their pharmacological properties, resulting in the candidate compound **12**, a potent and highly selective PARP/PI3K dual inhibitor. Compared to Olaparib, compound **12** exhibits a superior antiproliferative profile against BRCA-proficient MDA-MB-468 cells. In MDA-MB-468 cell-derived xenograft model, compound **12** displayed excellent antitumor efficacy at a dose of 50 mg/kg, which is considerably more efficacious than the single administration of Olaparib or BKM120. Furthermore, compound **12** displayed good metabolic stability and high safety. Taken together, these results suggest that compound **12** as a novel PARP/PI3K dual inhibitor is worthy for further study.

© 2020 Elsevier Masson SAS. All rights reserved.

1. Introduction

Triple negative breast cancer (TNBC) which characterized by deficient expression of estrogen, progesterone, and human epidermal growth factor receptor 2 receptors, is a particularly aggressive subtype of breast cancer with poorer prognosis and higher recurrence [1,2]. Current treatment options for TNBC are limited to chemotherapeutic regimens that are highly toxic and cannot be cured. Despite advances in targeted drugs [3–7], the treatment of TNBC still remains a major challenge in clinical practice. Cancer Genome Atlas revealed that the genomic alterations of TNBC included extensive copy number alterations, p53 mutations, phosphoinositide 3-kinase (PI3K) pathway activation, and deficiencies in DNA damage repair, such as homologous recombination (HR), which provided a rationale for the design of TNBC targeted therapy drugs [8,9].

BRCA1 and BRCA2 proteins are essential components of HR that

are recruited to damaged DNA for repairing of the double-strand breaks (DSBs) [10,11]. The loss or mutation of BRCA1/2 in breast epithelial cells disables DNA damage repair via HR, leading to genomic instability and predisposing patients to hereditary breast cancer [11]. Poly(ADP-ribose)polymerase (PARP) is a kind of nuclear enzyme which plays important roles in the repair of DNA single-strand breaks (SSBs) through the base excision repair (BER) pathway and non-homologous end joining (NHEJ) pathway [12]. When PARP is inhibited, unrepaired SSBs accumulate in BRCA-deficient cells and transform into DSBs that HR cannot repair, leading to continuous and lethal DNA damage [13–15]. Therefore, the loss of BRCA1/2 will result in HR deficiency and make cancer cells sensitive to PARP inhibitors.

Based on the concept of synthetic lethality, four PARP inhibitors, Olaparib [16,17], Rucaparib [18], Niraparib [19,20] and Talazoparib [21] have been approved to treat BRCA-mutant advanced ovarian cancer and metastatic breast cancer (Fig. 1). However, only a fraction of TNBC patients harbor BRCA mutations are benefit to this treatment, limiting the clinical application of PARP inhibitors. Meanwhile, the resistance caused by reversion of BRCA mutations and other mechanisms reduces the clinical efficacy of PARP inhibitors [22,23]. Therefore, development of advanced therapies for TNBC without BRCA mutation remains in high demand and challenging.

* Corresponding author. State Key Laboratory of Natural Medicines, China Pharmaceutical University, Nanjing, 210009, China.

** Corresponding author. State Key Laboratory of Natural Medicines, China Pharmaceutical University, Nanjing, 210009, China.

E-mail addresses: xyg@cpu.edu.cn (Y. Xu), zhuqihua@vip.126.com (Q. Zhu).

¹ Contributed equally.

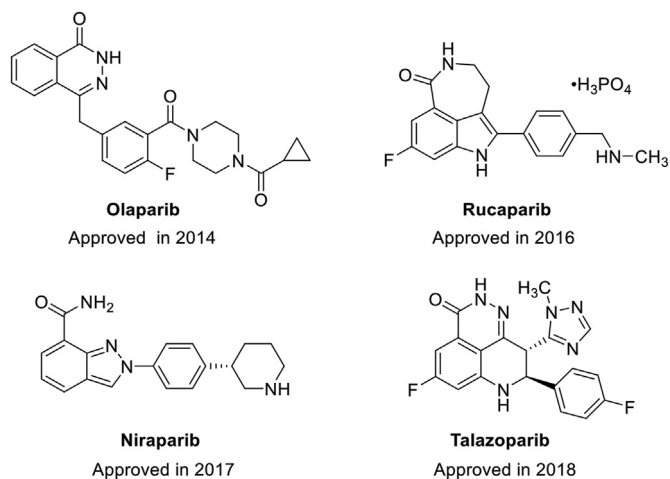


Fig. 1. Chemical structures of representative PARP inhibitors.

PI3K/AKT/mTOR pathway is aberrant activated in TNBC, which stabilizes and preserves DSB repair by interacting with the HR complex [24,25]. Thus, co-targeting of PARP and PI3K may be a promising chemotherapeutic strategy to treat BRCA-proficient TNBC. In 2012, Ibrahim and Juvekar independently found that PI3K inhibition impairs the expression of BRCA1/2 and sensitizes BRCA-proficient TNBC to PARP inhibitors, providing a rationale to combine PARP and PI3K inhibitors in the treatment of BRCA-proficient TNBC [26,27]. Based on these findings, a clinical trial with BKM120 and Olaparib is being initiated in patients with TNBC [28]. Despite the highly significant therapeutic relevance of drug combination therapy, it turned out to be considerably challenging due to complicated pharmacokinetics, dissimilar toxicity profiles, undesirable drug-drug interactions, as well as issues of patient compliance [29–31]. Thus, the design of dual-target or multi-target drugs becomes an effective strategy to overcome these drawbacks. Herein, we present the design, synthesis and biological evaluation of novel dual PARP/PI3K inhibitors based on the structural optimization of compound **1** [32]. And our medicinal chemistry efforts finally led to the discovery of a promising candidate **12**, which displayed good physicochemical properties, and potent *in vitro* and *in vivo* activities against BRCA-proficient TNBC (Fig. 2).

2. Results and discussion

2.1. Design of novel dual PARP/PI3K inhibitors

In our previous work, we have discovered a highly potent dual PARP/PI3K inhibitor through pharmacophore merging and scaffold hopping strategies, demonstrating that co-targeting PARP and PI3K with a single chemical entity is feasible [32]. As part of our ongoing program aiming at discovery of dual PARP/PI3K inhibitor with new structural type and improved druggable, we hypothesized that replacing the phthalazine moiety with a structurally smaller pharmacophore of PARP inhibitor could retain the potency and reduce the size of such hybrid compound for a favorable physicochemical and pharmacologic profile. Thus, compound **3** was designed by replacing the phthalazine moiety with benzofuran-7-carboxamide moiety which is a structurally smaller pharmacophore of PARP inhibitor (Fig. 1). A docking study was subsequently performed to verify the rationality of the design by analyzing the binding mode of compound **3** in the active sites of PARP-1 (PDB code 5DS3) [33] and PI3K α (PDB code 4JPS) [34]. As shown in Fig. 2, compound **3** can form three key hydrogen bonds with Ser904 and

Gly863, and π -stacking interactions with Tyr907. In addition, compound **3** can form a hydrogen bond with Val851 and three key hydrogen bonds with Asp810, Asp933 and Tyr836 (Fig. 3). The docking results showed that compound **3** fitted well in the active site pocket of PARP-1 and PI3K α , and formed efficient binding interactions with the key residues in the corresponding active site, indicating its potential to inhibit both PARP-1 and PI3K α .

2.2. Structure optimization and *in vitro* PARP-1/PI3K α inhibition assay

To validate the feasibility of our design, compound **3** was synthesized and evaluated for PARP-1 and PI3K α inhibitory activities *in vitro*. The results showed that compound **3** exhibited good PARP-1 and PI3K α inhibitory activity with the inhibition ratio more than 50% at 10 nM and 100 nM, respectively. Encouraged by this promising result, compound **3** was chosen as new lead compound for further optimization to find more potent dual PARP/PI3K inhibitors. Compounds (**4–11**) were designed and synthesized by varying the R¹ substituent and 1,3,5-triazine scaffold, and their PARP-1 and PI3K α inhibitory activities were summarized in Table 1. As expected, R¹ substituent had no significant effect on PARP-1 inhibitory activity, and most compounds exhibited potent PARP-1 inhibitory activity with the inhibition ratio more than 50% at 10 nM. However, PI3K α inhibitory activity was considerably depending on the R¹ substituent. The aromatic groups with a lower electron density showed better PI3K α inhibitory activity. For example, compounds **6–8** with a pyrimidine or pyridine ring showed stronger PI3K α inhibitory activity than compound **9** with a benzene ring, compound **10** with an indole ring and compound **11** with a benzimidazole ring (Table 1). In addition, we found that 1,3,5-triazine scaffold is more beneficial for PI3K α inhibition than pyrimidine scaffold. Overall consideration of PARP-1 and PI3K α inhibition ratio, compounds **6–8** were selected to evaluate the IC₅₀ values (Table 2). As a result, the structural optimization culminated in compound **8**, which remained potent and balanced PARP-1 and PI3K α inhibitory activities with the IC₅₀ values of 5.8 nM and 6.3 nM, respectively.

2.3. Physical and chemical property optimization

Although compound **8** displayed excellent *in vitro* inhibitory activity against PARP-1 and PI3K α , poor solubility and pharmacokinetic parameters profile hindered its further investigation. To improve its solubility, we tried to synthesis hydrochloride, tartrate and phosphate salts of **8**. However, there was little improvement in the solubility of these salts. We hypothesized that the addition of a hydrophilic group might be an effective way to increase its solubility. As a result, compound **13**, which incorporated a basic, solubilizing *N*-acetyl morpholine group on the amino of pyrimidine was designed. However, we failed to obtain this compound after several attempts of synthesis. To our delight, when introducing a hydrophilic group to compound **6**, the corresponding product **12** was successfully obtained (Fig. 4). Although its enzymes inhibitory activities were weaker than its parent compound **6**, the solubility of its hydrochloride was significantly increased (Table 3).

2.4. *In vitro* antiproliferative activity study

Considering their good inhibitory activities against PARP-1 and PI3K α , compounds **6** and **12** were selected to evaluate their antiproliferative activity against BRCA-proficient TNBC cells (MDA-MB-468). As shown in Table 4, compounds **6** and **12** both showed potent antiproliferative activity against MDA-MB-468 cells with the IC₅₀ values of 4.06 μ M and 1.40 μ M, respectively. In particular,

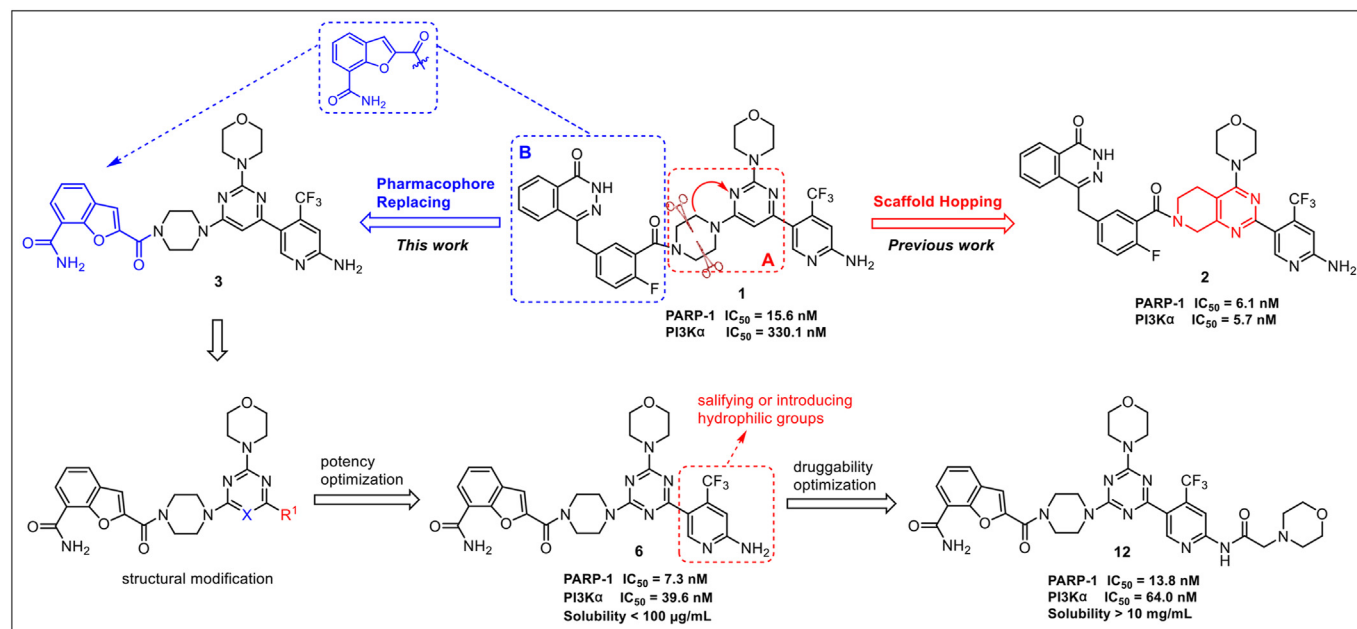


Fig. 2. Schematic illustration of the discovery of compound 12.

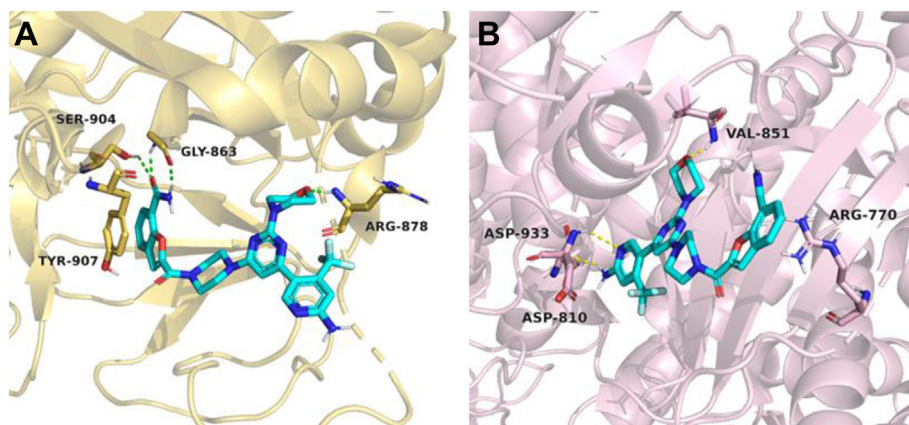


Fig. 3. Docking studies of compound 3 with PARP-1 (5DS3) and PI3K α (4JPS). Representation of the predicted binding mode of compound 3 in the active site of PARP-1 (A) and PI3K α (B). Hydrogen bonds are represented as yellow dotted lines. For clarity, nonpolar H atoms are not represented. (For interpretation of the references to color in this figure legend, the reader is referred to the Web version of this article.)

compound **12** showed much stronger antiproliferative activity than Olaparib against BRCA-proficient TNBC cells.

2.5. Effect on the expression of BRCA1/2

To verify whether BRCA1/2 was downregulated in MDA-MB-468 cancer cells after treating with PARP/PI3K dual inhibitor, the expression of BRCA1/2 at the mRNA level was measured by real-time PCR. As shown in Fig. 5, compound **12** displayed a stronger capability to downregulate the expression of BRCA1/2 at the mRNA level than Olaparib and BKM120, suggesting that compound **12** probably induced HR deficiency through the downregulation of BRCA1/2.

2.6. Apoptosis analysis

Further, to determine the effect of compound **12** on cell death, an apoptosis assay was conducted using Annexin-V by FACS

analysis in the MDA-MB-468 cell line. As shown in Fig. 6, compound **12** led to a significant increase in cell apoptosis compared to both single agent treatments and the combination of Olaparib and BKM120. The result suggested the superiority of PARP-1/PI3K dual inhibitors in inducing apoptosis of BRCA-proficient TNBC cells.

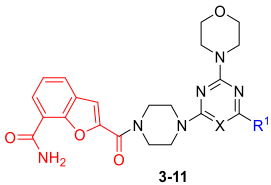
2.7. Metabolic stability study of compound 12

To evaluate the metabolic stability, compound **12** was incubated with liver microsomes of different species (mouse, rat, dog, monkey and human) for 1 h (Table 6). The results showed that compound **12** possessed good metabolic stability in all species, especially more stable in human liver microsomes (HLM).

2.8. Permeability study of compound 12

With good metabolic stability, the permeability and drug transport characteristics of compound **12** was investigated in a

Table 1
In vitro PARP-1 and PI3K α inhibitory activities of compounds **3–11**.



3-11

Compd	X	R ¹	Inhibition Ratio	
			PARP-1 (10 nM)	PI3K α (100 nM)
3	C		51%	80%
4	C		85%	60%
5	C		38%	26%
6	N		60%	77%
7	N		61%	79%
8	N		70%	86%
9	N		51%	5%
10	N		62%	8%
11	N		36%	29%
Olaparib			91%	ND
BKM120			ND	82%

Table 2
IC₅₀ values of representative compounds against PARP-1 and PI3K α .

Compd	IC ₅₀ (nM) ^a	
	PARP-1	PI3K α
6	7.3 ± 0.2	39.6 ± 1.3
7	10.8 ± 0.1	118.5 ± 2.5
8	5.8 ± 0.6	6.3 ± 0.9

^a The data are expressed as the mean ± SD from the dose-response curves of three independent experiments.

Caco-2 monolayer cell model (Table 7). The results demonstrated that compound **12** showed good membrane permeability with Papp (A-B) values more than 1 × 10⁻⁶ cm/s.

2.9. Toxicity study of compound **12**

To further evaluate the safety of compound **12** in vivo, additional maximum tolerated dose (MTD) determination tests was conducted. As shown in Table 8, no rats died and no significant weight loss was observed after single-dose treatment of 1000 mg/kg. Therefore, compound **12** exhibited an MTD values over 1000 mg/kg. Meanwhile, compound **12** exhibited very weak hERG inhibition with an IC₅₀ of 29.4 μ M (IC₅₀ > 10 μ M: very weak inhibition or no inhibition). All above results indicated that compound **12** exhibited high safety.

2.10. In vivo antitumor effects study

Based on the excellent enzymatic and antiproliferative activities of compound **12** in vitro, we then evaluated its antitumor activity in vivo in MDA-MB-468 xenograft mouse model. Compounds **12**, Olaparib, BKM120, and the combination of Olaparib and BKM120 were administered by intraperitoneal injection twice daily (BID) for 34 consecutive days. As shown in Fig. 7, compound **12** significantly suppressed the tumor growth at a dose of 50 mg/kg and it was well-tolerated with no mortality. The tumor suppression effects of compound **12** (TGI: 54.6%) was more effective than Olaparib (TGI: 28.5%) and BKM120 (TGI: 33.4%), and even the combination of Olaparib and BKM120 (TGI: 48.4%). It is also noteworthy that no significant weight fluctuations were observed during the whole process. The results suggest that dual PARP/PI3K inhibitor is superior to the single-target inhibitors in the antitumor efficacy against BRCA-proficient TNBC.

2.11. Kinase selectivity study

To demonstrate whether the compound has potential off-target effect, compound **12** was tested at a single concentration of 1 μ M against 374 kinases in the Reaction Biology Corporation (RBC) kinase panel (see Supporting Information). The results showed that compound **12** displayed weak inhibitory activities against 374 kinases at 1 μ M concentration (Fig. 8A and Table S1), demonstrating that compound **12** is a highly selective dual PARP/PI3K inhibitor. To further profile compound **12**'s selectivity against PARP and PI3K isoform, we tested its inhibitory activities against PARP-1/2 and four class I isoforms of PI3K. The results in Fig. 2B indicated that compound **12** possesses strong inhibitory effect on PARP-1/2 and PI3K α (Fig. 8B).

2.12. Chemistry

The starting material **13** underwent a replacement with a cyano, then hydrolysis of the cyano and ester gave intermediate **15**. The following condensation of **15** with **16** or **17** in the presence of PyBOP and DIPEA furnished intermediate **18** or **19**. Target compounds **3**, **4**, **6–10** and **12** were finally obtained by Suzuki coupling of **18** or **19** with the corresponding boric acid esters **20a–f** (Scheme 1).

The reaction of starting material **21** with **22** or **23** in the presence of K₂CO₃ gave intermediate **24** or **25**, which underwent substitution with *N*-Boc-piperazine and *N*-deprotection to give intermediate **28** or **29**. Compounds **5** and **11** were finally obtained by the condensation of **15** with **28** or **29** in the presence of PyBOP and DIPEA (Scheme 2).

3. Conclusions

In conclusion, to develop novel PARP/PI3K dual inhibitors, lead compound **3** was designed by replacing the phthalazine moiety of previous discovered PARP/PI3K dual inhibitor **1** with a benzofuran-

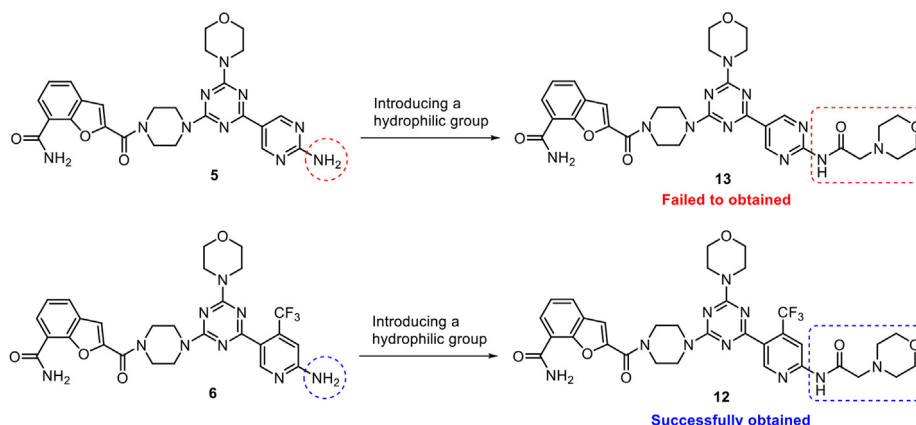


Fig. 4. Strategy to improve water solubility.

Table 3
Solubility and enzymes inhibitory activities of compounds **6** and **12**.

Compd	Solubility pH = 7	IC ₅₀ ±SD (nM)	
		PARP-1	PI3K α
6 · HCl	<100 μ g/mL	7.3 ± 0.2	39.6 ± 1.3
12 · HCl	>10 mg/mL	13.8 ± 1.9	64.0 ± 2.5

Table 4
In vitro antiproliferative activity of compounds **6** and **12**.

Compd	IC ₅₀ ±SD (μ M) ^a
	MDA-MB-468
6	4.06 ± 0.49
12	1.40 ± 0.13
Olaparib	13.72 ± 2.52
BKM120	3.97 ± 0.28

^a The data are shown as the mean ± SD from the dose-response curves of three independent experiments.

7-carboxamide moiety. Subsequent structural optimization leading to the candidate compound **12**, which showed potent and highly selective inhibitory activities against PARP and PI3K with IC₅₀ values of 13.8/6.2 nM (PARP1/2) and 64 nM (PI3K α), respectively. Moreover, compound **12** showed much stronger antiproliferative activity than Olaparib against BRCA-proficient TNBC cells. In MDA-

MB-468 cell-derived xenograft model, compound **12** displayed excellent antitumor efficacy at a dose of 50 mg/kg, which is considerably more efficacious than the single administration of Olaparib or BKM120. Compound **12** also possessed good metabolic stability and high safety. In view of its encouraging in vitro and in vivo properties, compound **12** as a novel PARP/PI3K dual inhibitor is worthy of further profiling and is currently under preclinical study.

4. Experimental sections

4.1. Materials and physical measurements

All cell culture reagents were purchased from Gibco (Invitrogen, USA). 3-(4,5-dimethylthiazol-2-yl)-2,5-diphenyltetrazolium bromide (MTT), STZ, wortmannin, SB216763 and chloroquine were purchased from Sigma-Aldrich company (USA). All chemical reagents were purchased from Sinopharm Chemical Reagent Co., Ltd. (China), Alfa Aesar, Adamas-beta, J&K and TCI. All solvents were used without further purifications. Reaction progress was monitored using analytical thin layer chromatography (TLC) on pre-coated silica gel GF254 (Yantai, China) plates and the spots were detected under UV light (254 nm). Column chromatography was performed on silica gel (200–300 mesh) from Yantai (China). Melting point were recorded on a WRS-1B melting point apparatus and uncorrected. ¹H NMR and ¹³C NMR spectra were measured in

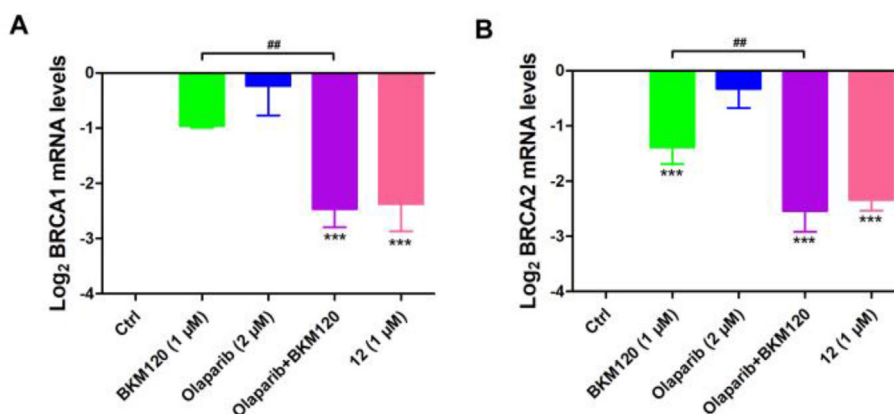


Fig. 5. Effects of BKM120, Olaparib, BKM120 (1 μ M) + Olaparib (2 μ M), compound **12** on BRCA1 and BRCA2 expression in MDA-MB-468 cancer cells treated with the indicated compounds. Gene expression was normalized to GAPDH. The data are shown as the mean ± SD of three independent experiments. ***p < 0.001 vs. control.

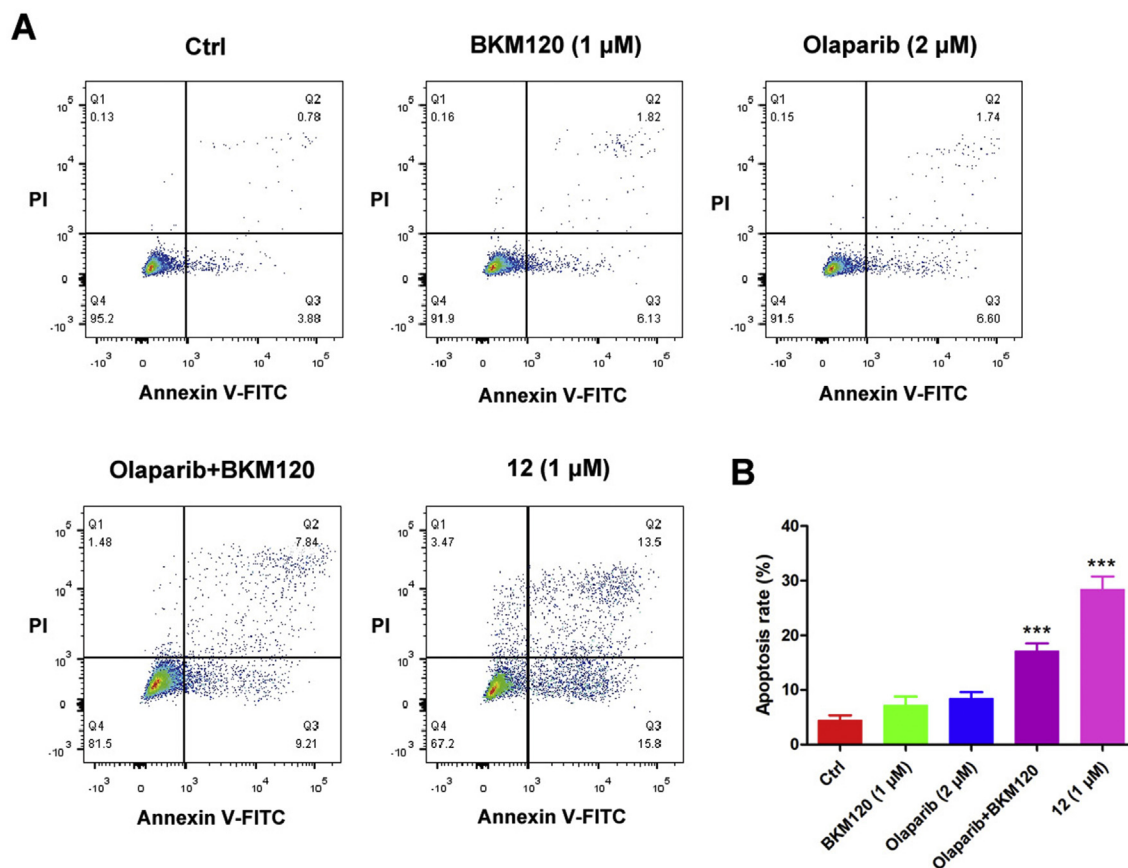


Fig. 6. Effects of BKM120, Olaparib, BKM120 (1 μM) + Olaparib (2 μM) and compound **12** to induce apoptosis of MDA-MB-468 cells. (A) MDA-MB-468 cells were treated with the indicated concentrations of compounds for 72 h. The apoptosis rate was measured using flow cytometry. (B) The percentage of cells in each population. The data are shown as the mean ± SD of three independent experiments. *** $p < 0.001$ vs. control.

Table 6

Evaluation of the metabolic stability of different species liver microsomes.

Species	k (min^{-1}) ^a	$T_{1/2}$ (min) ^b	CL_{int} ($\mu\text{L}/\text{min}/\text{mg}$) ^c
Human	0.00734	107	14.7
Monkey	0.0153	59.1	30.7
Dog	0.0147	47.3	29.3
Rat	0.0165	42.2	32.9
Mouse	0.0398	17.4	79.7

^a k is the drug elimination rate constant

^b $T_{1/2}$ is the elimination half-life.

^c CL_{int} is the intrinsic clearance.

Table 7

Measurement of bidirectional Papp and efflux ratio of compound **12**^a.

Direction	Recovery (%)	P_{app} (10^{-6} cm/s) ^b	Efflux Ratio
A to B	67.3	8.42	2.6
B to A	99.9	22.1	

^a Test compound concentration: 5 μM; incubation time: 120 min.

^b Values are reported as the mean of two experiments.

DMSO- d_6 or CDCl_3 solutions using an AVANCE III 300 or 600 spectrometer. Chemical shifts are reported in δ scale (ppm) relative to internal TMS, J values are given in Hertz, and spin multiplicities are expressed as s (singlet), d (doublet), t (triplet), or m (multiplet). Low and high-resolution mass spectra were obtained in the ESI mode.

Table 8

Weight changes of rats^a treated with a single dose^b of 1000 mg/kg.

Compd	weight (g) ^c			
	adaptation period	Day 2	Day 4	Day 7
Control	258 ± 13	273 ± 15	280 ± 12	298 ± 14
12	256 ± 11	267 ± 14	272 ± 10	281 ± 12*

* $p < 0.05$ vs. control, ** $p < 0.01$.

^a Sprague–Dawley rat; $n = 6$ animals, half male and half female.

^b Oral administration once a day.

^c Values presented are the mean of six independent mice.

4.2. Chemistry

4.2.1. General procedure for the synthesis of compounds **3**, **4**, **6–10**, **12**

To a solution of compound **13** (9.30 g, 36.46 mmol) in DMF (100 mL) was added $\text{Zn}(\text{CN})_2$ (8.56 g, 72.92 mmol) and $\text{Pd}(\text{PPh}_3)_4$ (2.10 g, 1.82 mmol). The suspension was heated with stirring under a nitrogen atmosphere at 80 °C for 6–8 h. The reaction was checked by TLC. After completion of the reaction, the mixture was cooled to room temperature and filtered. The filtrate was poured into water (300 mL) and stirred for 10 min. The precipitate was filtered and washed with water, then dried under vacuum. The crude product was purified by silica gel column chromatography (PE/EtOAc = 50:1 to 20:1) to give intermediate **14** as white solid (4.70 g, 64.0% yield). m.p.: 130–132 °C. ^1H NMR (300 MHz, CDCl_3) δ (ppm): 7.97 (1H, dd, $J = 8.0, 1.0$ Hz, ArH), 7.79 (1H, dd, $J = 7.6, 1.0$ Hz, ArH), 7.62 (1H, s,

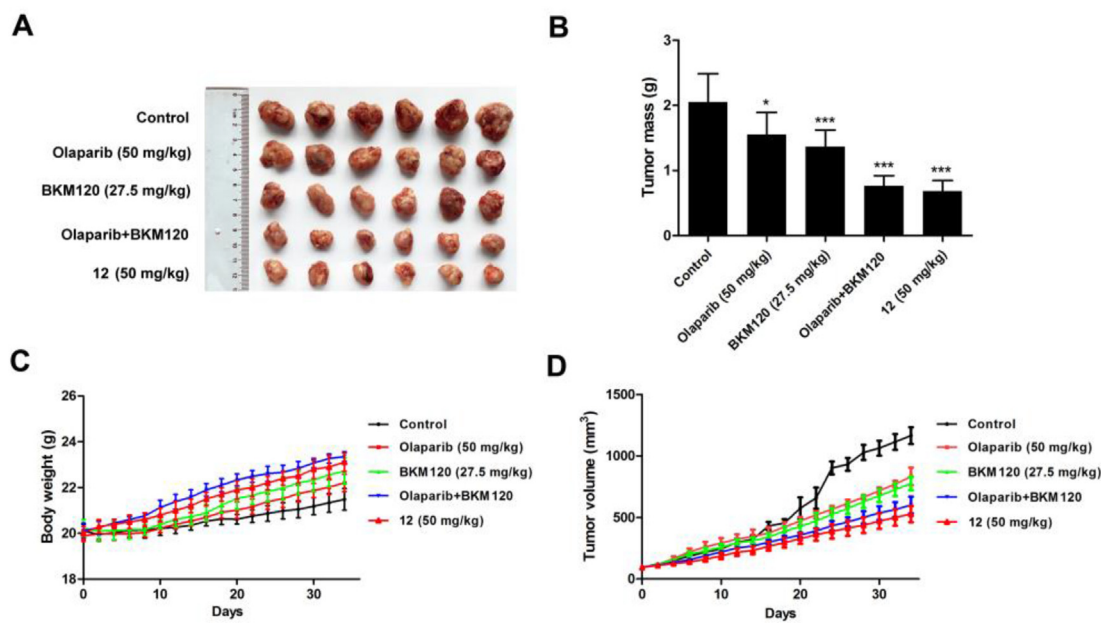


Fig. 7. Effects of Olaparib, BKM120, Olaparib (50 mg/kg) + BKM120 (27.5 mg/kg), and compound **12** treatment on the tumorigenicity of MDA-MB-468 cells in vivo. (A) The resulting tumors excised from the animals after treatment. (B) The tumor masses for six groups of animals were compared, and each histogram represents the Mean \pm S.D. of 6 mice. * $p < 0.05$ vs. control; *** $p < 0.001$. (C) The nude mouse body weight was measured every 2 days. (D) The tumor volumes of the nude mice were measured and calculated once every 2 days.

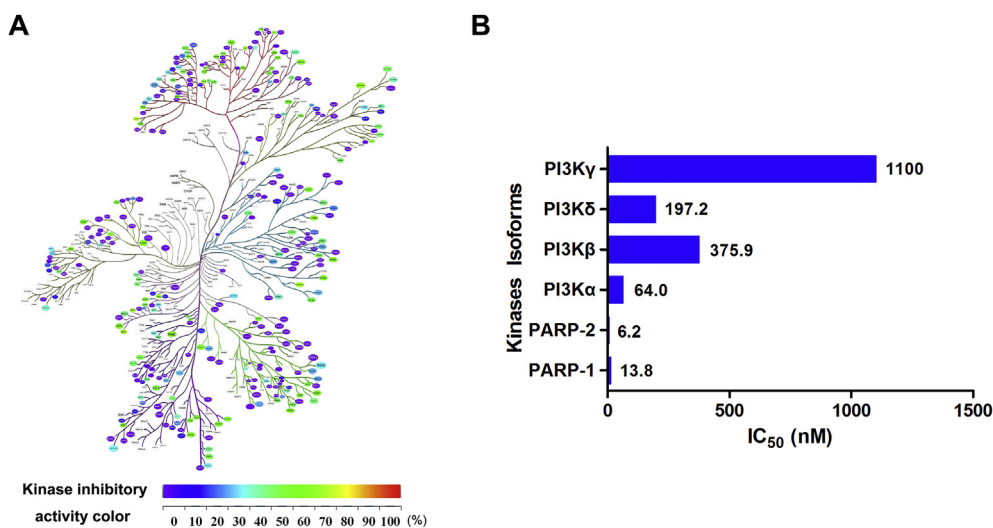


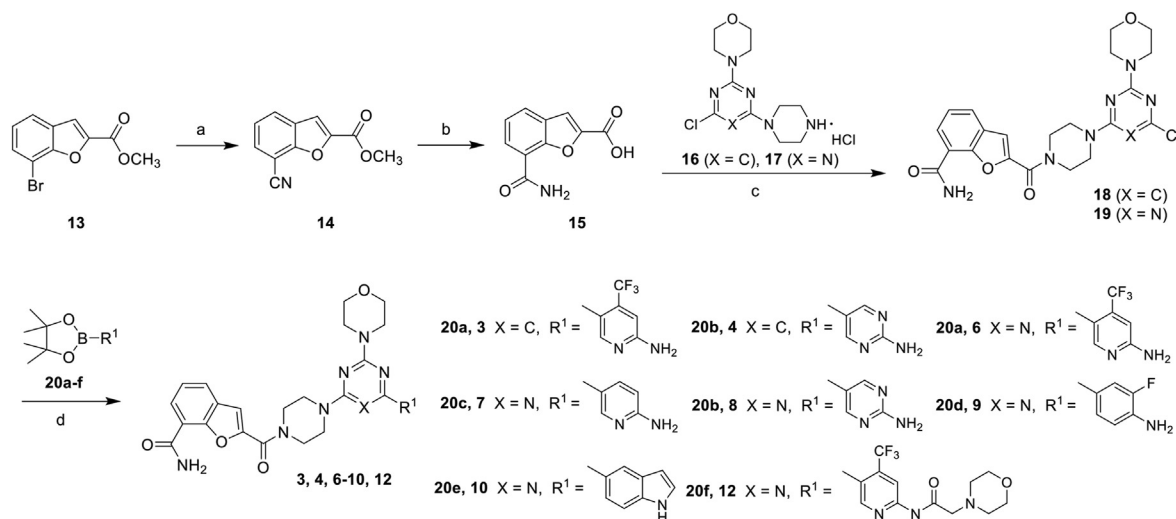
Fig. 8. (A) Kinase selectivity profile of compound **12** as shown by an RBC kinase panel screen against 374 kinases assayed at 1 μ M in duplicate. Compound selectivity is represented in a dendrogram view of the human kinome phylogenetic tree. The color code for inhibition is indicated. (B) Inhibitory activity of compound **12** against PARP-1/2 and four isoforms of PI3K. (For interpretation of the references to color in this figure legend, the reader is referred to the Web version of this article.)

ArH), 7.43 (1H, t, $J = 7.8$ Hz, ArH), 4.02 (3H, s, CH₃).

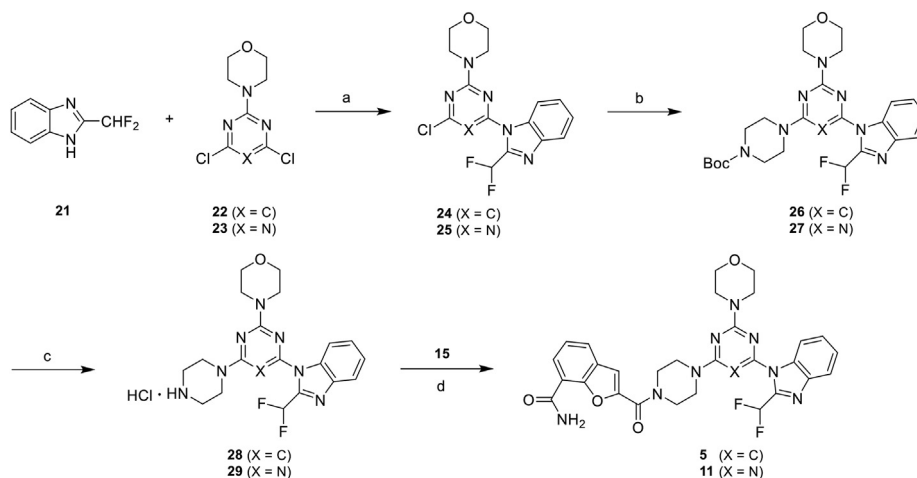
To a solution of intermediate **14** (4.70 g, 23.36 mmol) in MeOH (50 mL) was added 30% H₂O₂ (16 mL), 1 mol/L NaOH (47 mL). The mixture was heated with stirring at 40 °C for 1 h. After completion of the reaction, the mixture was cooled to room temperature and added 2 mol/L HCl to adjust the pH to 2. The precipitate was filtered, washed with water and dried under vacuum to give **15** as white solid (4.50 g, 93.9% yield). m.p.: 178–180 °C. ¹H NMR (300 MHz, DMSO-*d*₆) δ (ppm): 13.77 (1H, s, COOH), 7.92 (1H, d, $J = 7.5$ Hz, ArH), 7.85 (1H, s, 1/2CONH₂), 7.83 (1H, d, $J = 7.6$ Hz, ArH), 7.74 (1H, s, ArH), 7.66 (1H, s, 1/2CONH₂), 7.42 (1H, t, $J = 7.4$ Hz, ArH).

Intermediate **15** (1.35 g, 6.58 mmol), **17** (2.12 g, 6.60 mmol) and

PyBOP (4.12 g, 7.92 mmol) were dissolved in DMF (50 mL), followed by the addition of DIPEA (3.82 mL, 23.10 mmol). The mixture was stirred at 25 °C for 6 h. After completion, the solution was poured into water (150 mL) and stirred for 10 min. The precipitate was filtered and washed with water, then dried under vacuum. The crude product was purified by silica gel column chromatography (DCM/MeOH = 80:1 to 30:1) to give compound **19** as white solid (2.50 g, 80.4% yield). m.p.: 142–144 °C. ¹H NMR (300 MHz, DMSO-*d*₆) δ (ppm): 7.94 (1H, d, $J = 7.8$ Hz, ArH), 7.86 (1H, d, $J = 7.1$ Hz, ArH), 7.84 (1H, s, 1/2CONH₂), 7.77 (1H, s, 1/2CONH₂), 7.58 (1H, s, ArH), 7.46 (1H, t, $J = 7.7$ Hz, ArH), 3.90–3.66 (16H, m, 6CH₂N, 2CH₂O). The synthesis methods of intermediate **18** refer to that of



Scheme 1. Reagents and conditions: (a) $\text{Zn}(\text{CN})_2$, $\text{Pd}(\text{PPh}_3)_4$, DMF, N_2 , 80 °C, 6 h; (b) 1 mol/L NaOH, H_2O , MeOH, 40 °C, 1 h; (c) PyBOP, DIPEA, DMF, 25 °C, 6 h; (d) $\text{Pd}(\text{PPh}_3)_4$, K_2CO_3 , dioxane/ H_2O , reflux, N_2 , 8 h.



Scheme 2. Reagents and conditions: (a) K_2CO_3 , DMF, 25 °C, 4 h; (b) *N*-Boc-piperazine, K_2CO_3 , acetone, 30 °C, 10 h; (c) HCl/EtOAc, 25 °C, 4 h; (d) PyBOP, DIEA, DMF, 25 °C, 8 h.

intermediate **19**.

To a solution of intermediate **18** or **19** (0.64 mmol) in dioxane (20 mL) was added the corresponding boric acid esters (0.70 mmol), $\text{Pd}(\text{PPh}_3)_4$ (0.06 mmol) and K_2CO_3 (2.56 mmol) which was dissolved in water (2 mL). The suspension was heated with stirring under a nitrogen atmosphere at 100 °C for 6–8 h. The reaction was checked by TLC. After completion, the mixture was cooled to room temperature and evaporated under vacuum. The residue was partitioned between EtOAc (20 mL) and water (20 mL), and the water phase was extracted two times with the same volume of EtOAc. The combined organic phase was washed with water and brine, dried over Na_2SO_4 overnight, and the solvent was evaporated under vacuum. The crude products were purified by silica gel column chromatography (DCM/MeOH = 100:1 to 20:1) to yield the target compounds **3**, **4**, **6–10**, **12**.

4.2.2. 2-(4-(6-(6-amino-4-(trifluoromethyl)pyridin-3-yl)-2-morpholinopyrimidin-4-yl)piperazine-1-carbonyl)benzofuran-7-carboxamide (**3**)

The product was light yellow solid, 45.8% yield, m.p.: 208–210 °C. ^1H NMR (300 MHz, $\text{DMSO}-d_6$) δ (ppm): 8.17 (1H, s,

ArH), 7.91 (1H, d, $J = 8.3$ Hz, ArH), 7.82 (1H, d, $J = 7.1$ Hz, ArH), 7.79 (1H, s, 1/2CONH₂), 7.72 (1H, s, 1/2CONH₂), 7.53 (1H, s, ArH), 7.42 (1H, t, $J = 7.6$ Hz, ArH), 6.82 (1H, s, ArH), 6.73 (2H, s, NH₂), 6.25 (1H, s, ArH), 4.03–3.59 (16H, m, 6CH₂N, 2CH₂O). ^{13}C NMR (75 MHz, $\text{DMSO}-d_6$) δ (ppm): 165.3, 162.8, 162.7, 160.3, 159.9, 159.0, 150.8, 150.3, 148.2, 136.0, 127.6, 126.8, 125.9, 124.8, 123.7, 121.3, 119.1, 110.9, 104.6, 92.0, 65.8, 49.8, 43.8, 43.3. HRMS (ESI): m/z [$\text{M}+\text{H}$]⁺. Calcd for $\text{C}_{28}\text{H}_{27}\text{F}_3\text{N}_8\text{O}_4$: 597.2180; Found: 597.2177. IR (cm^{-1}): 3481.4, 3423.6, 3323.0, 3212.3, 2858.5, 1683.7, 1627.1, 1571.9, 1554.7, 1535.1, 1513.8, 1434.4, 1408.7, 1373.3, 1261.1, 1241.4, 1195.2, 1175.1, 1153.0, 1135.5, 1116.9, 1008.5, 994.4, 975.0, 962.6, 938.8, 872.1, 838.7, 816.8, 742.9, 670.0, 500.9.

4.2.3. 2-(4-(2'-amino-2-morpholino-[4,5'-bipyrimidin]-6-yl)piperazine-1-carbonyl)benzofuran-7-carboxamide (**4**)

The product was light yellow solid, 47.2% yield, m.p.: >250 °C. ^1H NMR (300 MHz, $\text{DMSO}-d_6$) δ (ppm): 8.99 (2H, s, ArH), 7.94 (1H, dd, $J = 7.8, 1.3$ Hz, ArH), 7.89–7.82 (2H, m, ArH, 1/2CONH₂), 7.76 (1H, s, 1/2CONH₂), 7.57 (1H, s, ArH), 7.46 (1H, t, $J = 7.7$ Hz, ArH), 7.09 (2H, s, NH₂), 6.66 (1H, s, ArH), 3.95–3.88 (8H, m, 4CH₂N), 3.72–3.64 (8H, m, 2CH₂N, 2CH₂O). ^{13}C NMR (150 MHz, $\text{DMSO}-d_6$) δ (ppm): 170.3,

169.3, 168.5, 165.9, 164.6, 163.9, 162.2, 162.0, 156.0, 154.0, 132.9, 131.8, 130.6, 128.8, 125.1, 125.0, 116.1, 91.8, 71.1, 49.2, 45.2. HRMS (ESI): m/z $[M+H]^+$. Calcd for $C_{26}H_{27}N_9O_4$: 530.2259; Found: 530.2250. IR (cm^{-1}): 3444.4, 3320.9, 3165.5, 2955.1, 2849.1, 2359.9, 1644.8, 1584.2, 1562.0, 1477.7, 1433.3, 1418.5, 1389.7, 1361.7, 1267.5, 1251.5, 1228.2, 1212.8, 1192.8, 1180.1, 1110.0, 1000.8, 973.9, 934.8, 880.9, 807.8, 734.3, 556.3, 532.6.

4.2.4. 2-(4-(4-(6-amino-4-(trifluoromethyl)pyridin-3-yl)-6-morpholino-1,3,5-triazin-2-yl)-piperazine-1-carbonyl)benzofuran-7-carboxamide (**6**)

The product was off-white solid, 48.4% yield, m.p.: >250 °C. HPLC: 98.06%. 1H NMR (300 MHz, DMSO- d_6) δ (ppm): 8.62 (1H, s, ArH), 7.92 (1H, d, J = 7.8 Hz, ArH), 7.83 (1H, d, J = 7.4 Hz, ArH), 7.77 (1H, s, 1/2CONH $_2$), 7.71 (1H, s, 1/2CONH $_2$), 7.55 (1H, s, ArH), 7.43 (1H, t, J = 7.7 Hz, ArH), 6.94 (2H, s, NH $_2$), 6.83 (1H, s, ArH), 3.92–3.65 (16H, m, 6CH $_2$ N, 2CH $_2$ O). ^{13}C NMR (75 MHz, DMSO- d_6) δ (ppm): 174.2, 169.8, 168.8, 165.9, 163.4, 157.2, 155.6, 153.4, 140.6, 132.4, 131.4, 130.1, 129.6, 128.3, 125.9, 124.6, 123.4, 115.8, 109.4, 70.6, 59.6, 47.9, 47.2. HRMS (ESI): m/z $[M+H]^+$. Calcd for $C_{27}H_{26}F_3N_9O_4$: 598.2133; Found: 598.2136. IR (cm^{-1}): 3422.6, 3207.6, 2854.9, 2361.1, 1682.4, 1649.3, 1622.2, 1560.6, 1525.2, 1484.9, 1437.5, 1420.0, 1389.8, 1365.9, 1274.2, 1259.8, 1227.1, 1166.4, 1128.41, 1056.3, 1001.8, 981.3, 963.4, 938.6, 924.0, 861.7, 813.6, 746.9, 677.7, 545.3.

4.2.5. 2-(4-(4-(6-aminopyridin-3-yl)-6-morpholino-1,3,5-triazin-2-yl)piperazine-1-carbonyl)-benzofuran-7-carboxamide (**7**)

The product was light yellow solid, 46.0% yield, m.p.: >250 °C. 1H NMR (300 MHz, DMSO- d_6) δ (ppm): 8.88 (1H, s, ArH), 8.34 (1H, d, J = 7.7 Hz, ArH), 7.90 (1H, d, J = 7.8 Hz, ArH), 7.82 (1H, s, ArH), 7.80 (1H, s, 1/2CONH $_2$), 7.75 (1H, s, 1/2CONH $_2$), 7.55 (1H, s, ArH), 7.42 (1H, t, J = 7.6 Hz, ArH), 7.06 (2H, s, NH $_2$), 6.62 (1H, d, J = 8.6 Hz, ArH), 4.00–3.57 (16H, m, 6CH $_2$ N, 2CH $_2$ O). ^{13}C NMR (75 MHz, DMSO- d_6) δ (ppm): 168.6, 165.0, 164.2, 161.9, 158.6, 150.8, 149.6, 148.7, 136.6, 131.4, 127.6, 126.6, 125.4, 123.6, 120.1, 119.9, 111.0, 106.9, 66.0, 43.2, 28.9, 26.5. HRMS (ESI): m/z $[M+H]^+$. Calcd for $C_{26}H_{27}N_9O_4$: 530.2259; Found: 530.2252. IR (cm^{-1}): 3458.8, 3376.6, 3183.6, 2920.8, 2850.6, 2361.0, 1683.0, 1628.4, 1569.8, 1532.6, 1519.9, 1487.1, 1436.2, 1419.3, 1388.4, 1364.3, 1261.9, 1225.7, 1178.6, 1154.2, 1118.2, 1017.1, 1001.1, 976.4, 940.8, 854.0, 814.2, 742.3, 543.0, 516.8, 490.7, 458.9, 409.1.

4.2.6. 2-(4-(4-(2-aminopyrimidin-5-yl)-6-morpholino-1,3,5-triazin-2-yl)piperazine-1-carbonyl)-benzofuran-7-carboxamide (**8**)

The product was white solid, 59.4% yield, m.p.: >250 °C. 1H NMR (300 MHz, DMSO- d_6) δ (ppm): 9.06 (2H, s, ArH), 7.90 (1H, d, J = 7.3 Hz, ArH), 7.82 (1H, s, 1/2CONH $_2$), 7.81 (1H, d, J = 5.4 Hz, ArH), 7.74 (1H, s, 1/2CONH $_2$), 7.55 (1H, s, ArH), 7.42 (1H, t, J = 7.1 Hz, ArH), 7.30 (2H, s, NH $_2$), 4.00–3.64 (16H, m, 6CH $_2$ N, 2CH $_2$ O). ^{13}C NMR (75 MHz, DMSO- d_6) δ (ppm): 170.8, 169.8, 168.6, 165.8, 163.4, 162.4, 155.6, 153.4, 147.6, 132.4, 131.4, 130.1, 128.3, 124.6, 123.3, 115.8, 70.7, 51.1, 48.0, 47.4. HRMS (ESI): m/z $[M+H]^+$. Calcd for $C_{25}H_{26}N_{10}O_4$: 531.2211; Found: 531.2209. IR (cm^{-1}): 3478.7, 2860.0, 2359.8, 1660.8, 1631.6, 1563.0, 1509.0, 1440.3, 1420.6, 1362.3, 1329.8, 1265.2, 1233.4, 1113.8, 1068.6, 1001.0, 977.5, 873.1, 856.3, 811.61, 783.6, 755.0, 658.7, 624.5, 543.1, 511.5, 469.0.

4.2.7. 2-(4-(4-(4-amino-3-fluorophenyl)-6-morpholino-1,3,5-triazin-2-yl)piperazine-1-carbonyl)-benzofuran-7-carboxamide (**9**)

The product was light yellow solid, 48.6% yield, m.p.: >250 °C. 1H NMR (300 MHz, DMSO- d_6) δ (ppm): 7.96–7.91 (3H, m, ArH), 7.84 (1H, d, J = 7.2 Hz, ArH), 7.80 (1H, s, 1/2CONH $_2$), 7.73 (1H, s, 1/2CONH $_2$), 7.56 (1H, s, ArH), 7.44 (1H, t, J = 7.7 Hz, ArH), 6.80 (1H, t, J = 8.9 Hz, ArH), 5.78 (2H, s, NH $_2$), 4.02–3.62 (16H, m, 6CH $_2$ N, 2CH $_2$ O). ^{13}C NMR (75 MHz, DMSO- d_6) δ (ppm): 168.7, 165.3, 164.3,

159.0, 150.8, 148.1, 139.6, 127.6, 126.8, 125.97, 125.1, 124.3, 123.8, 121.6, 119.1, 114.9, 114.5, 114.3, 111.1, 72.8, 65.9, 43.1, 42.4. HRMS (ESI): m/z $[M+H]^+$. Calcd for $C_{27}H_{27}FN_8O_4$: 547.2212; Found: 547.2211. IR (cm^{-1}): 3480.8, 3398.5, 3340.8, 3237.9, 2958.7, 2856.8, 1667.2, 1624.5, 1548.0, 1517.6, 1435.9, 1385.1, 1305.2, 1280.0, 1264.0, 1233.3, 1219.47, 1168.9, 1111.0, 1002.7, 983.4, 944.6, 913.0, 809.2, 770.7, 737.1.

4.2.8. 2-(4-(4-(1H-indol-5-yl)-6-morpholino-1,3,5-triazin-2-yl)piperazine-1-carbonyl)benzofuran-7-carboxamide (**10**)

The product was light yellow solid, 45.2% yield, m.p.: 164–166 °C. HPLC: 99.53%. 1H NMR (300 MHz, DMSO- d_6) δ (ppm): 11.35 (1H, s, NH), 8.70 (1H, s, ArH), 8.22 (1H, d, J = 8.8 Hz, ArH), 7.95 (1H, d, J = 7.8 Hz, ArH), 7.90–7.84 (2H, m, ArH, 1/2CONH $_2$), 7.79 (1H, s, 1/2CONH $_2$), 7.60 (1H, s, ArH), 7.51–7.42 (3H, m, ArH), 6.60 (1H, s, ArH), 4.12–3.84 (12H, m, 4CH $_2$ N, 2CH $_2$ O), 3.72–3.63 (4H, m, 2CH $_2$ N). ^{13}C NMR (75 MHz, DMSO- d_6) δ (ppm): 171.1, 165.6, 165.1, 165.0, 159.1, 151.4, 149.2, 138.6, 128.1, 128.0, 127.8, 127.2, 126.8, 125.9, 124.1, 122.0, 121.6, 120.4, 111.6, 111.3, 102.6, 74.0, 66.5, 55.3, 43.7. HRMS (ESI): m/z $[M+H]^+$. Calcd for $C_{29}H_{28}N_8O_4$: 553.2306; Found: 553.2306. IR (cm^{-1}): 3396.6, 2852.8, 2355.1, 1676.0, 1618.6, 1542.7, 1519.9, 1485.1, 1434.5, 1384.8, 1364.1, 1346.5, 1275.3, 1260.1, 1228.2, 1170.1, 1111.0, 1067.7, 1000.1, 979.46, 806.6, 770.7, 739.6, 716.7, 542.1, 429.0.

4.2.9. 2-(4-(4-morpholino-6-(6-(2-morpholinoacetamido)-4-(trifluoromethyl)pyridin-3-yl)-1,3,5-triazin-2-yl)piperazine-1-carbonyl)benzofuran-7-carboxamide (**12**)

The product was light yellow solid, 64.7% yield, m.p.: 163–165 °C. HPLC: 99.40%. 1H NMR (300 MHz, DMSO- d_6) δ (ppm): 10.78 (1H, s, NH), 8.93 (1H, s, ArH), 8.58 (1H, s, ArH), 7.94 (1H, dd, J = 7.8, 1.3 Hz, ArH), 7.90–7.77 (3H, m, ArH, CONH $_2$), 7.59 (1H, s, ArH), 7.45 (1H, t, J = 7.7 Hz, ArH), 3.99–3.77 (12H, m, 2CH $_2$ N, 4CH $_2$ O), 3.71–3.61 (8H, m, 4CH $_2$ N), 3.32 (2H, s, COCH $_2$ N), 2.58 (4H, t, J = 4.5 Hz, 2CH $_2$ N). ^{13}C NMR (150 MHz, DMSO- d_6) δ (ppm): 175.0, 174.0, 170.3, 169.1, 163.9, 158.2, 156.4, 156.1, 153.8, 141.9, 132.8, 132.3, 131.9, 131.8, 130.67, 128.8, 126.9, 125.1, 116.3, 114.5, 71.4, 71.1, 66.5, 58.2, 48.5, 48.3, 45.2. HRMS (ESI): m/z $[M+H]^+$. Calcd for $C_{33}H_{36}F_3N_{10}O_6$: 725.2766; Found: 725.2766. IR (cm^{-1}): 3446.2, 2928.5, 2862.3, 2360.8, 1708.2, 1629.3, 1585.4, 1510.5, 1438.8, 1383.9, 1351.58, 1259.9, 1227.9, 1170.9, 1123.1, 1067.4, 1000.5, 979.1, 854.9, 759.7, 669.6.

4.2.10. General procedure for the synthesis of compounds **5** and **11**

Intermediate **21** (500 mg, 2.97 mmol), **22** (700 mg, 2.99 mmol) and K_2CO_3 (411 mg, 2.97 mmol) were dissolved in DMF (25 mL). The mixture was stirred at 100 °C for 8 h. The reaction was checked by TLC. After completion of the reaction, the mixture was cooled to room temperature and then poured into water (80 mL). The precipitate was filtered and washed with water, then dried under vacuum. The crude product was purified by silica gel column chromatography (PE/EtOAc = 50:1 to 20:1) to give intermediate **24** as white solid (1.00 g, 91.7% yield), m.p.: 197–200 °C. 1H NMR (300 MHz, DMSO- d_6) δ (ppm): 8.31 (1H, d, J = 8.1 Hz, ArH), 7.86 (1H, d, J = 7.7 Hz, ArH), 7.69 (1H, t, J = 53.6 Hz, CHF $_2$), 7.55–7.42 (2H, m, ArH), 7.09 (1H, s, ArH), 3.74 (8H, brs, 2CH $_2$ O, 2CH $_2$ N).

Intermediate **24** (1.00 g, 2.73 mmol), *N*-Boc-piperazine (0.54 g, 2.87 mmol) and K_2CO_3 (0.57 g, 4.09 mmol) were dissolved in DMF (25 mL). The mixture was stirred at 80 °C for 10 h. The reaction was checked by TLC. After completion of the reaction, the mixture was cooled to room temperature and then poured into water (80 mL). The precipitate was filtered and washed with water, then dried under vacuum. The crude product was purified by silica gel column chromatography (PE/EtOAc = 30:1 to 5:1) to give intermediate **26** as white solid (1.25 g, 88.7% yield), m.p.: 195–198 °C. 1H NMR

(300 MHz, CDCl₃) δ (ppm): 8.22 (1H, d, J = 7.1 Hz, ArH), 7.90 (1H, d, J = 7.1 Hz, ArH), 7.51 (1H, t, J = 53.6 Hz, CHF₂), 7.44–7.35 (2H, m, ArH), 5.52 (1H, s, ArH), 3.84–3.81 (4H, m, 2CH₂O), 3.65–3.57 (12H, m, 6CH₂N).

To a solution of compound **26** (1.20 g, 2.33 mmol) in EtOAc (10 mL) was added the EtOAc solution of HCl (5 mL). The mixture was stirred at 25 °C for 5 h. The reaction was checked by TLC. After completion of the reaction, the precipitate was filtered and washed with EtOAc, then dried under vacuum to give intermediate **28** as white solid (0.89 g, 84.8% yield). m.p.: 196–198 °C. ¹H NMR (300 MHz, DMSO-*d*₆) δ (ppm): 9.10 (2H, brs, NH, HCl), 8.20 (1H, d, J = 8.1 Hz, ArH), 7.82 (1H, d, J = 7.7 Hz, ArH), 7.68 (1H, t, J = 53.1 Hz, CHF₂), 7.49–7.39 (2H, m, ArH), 6.08 (1H, s, ArH), 3.88–3.65 (12H, m, 2CH₂O, 4CH₂N), 3.18 (4H, brs, 2CH₂N).

Intermediate **21** (1.43 g, 8.50 mmol), **23** (2.00 g, 8.51 mmol) and K₂CO₃ (1.18 g, 8.51 mmol) were dissolved in DMF (25 mL). The mixture was stirred at 25 °C for 4 h. The reaction was checked by TLC. After completion of the reaction, the mixture was cooled to room temperature and then poured into water (80 mL). The precipitate was filtered and washed with water, then dried under vacuum to give intermediate **25** as white solid (2.70 g, 86.5% yield). m.p.: 244–247 °C. ¹H NMR (300 MHz, CDCl₃) δ (ppm): 8.44 (1H, d, J = 7.7 Hz, ArH), 7.91 (1H, d, J = 7.5 Hz, ArH), 7.59 (1H, t, J = 53.4 Hz, CHF₂), 7.53–7.43 (2H, m, ArH), 4.02–3.95 (4H, m, CH₂), 3.87–3.81 (4H, m, CH₂).

Intermediate **25** (2.70 g, 7.36 mmol), *N*-Boc-piperazine (1.44 g, 7.73 mmol) and K₂CO₃ (1.53 g, 11.04 mmol) were dissolved in acetone (50 mL). The mixture was stirred at 30 °C for 8 h. The reaction was checked by TLC. After completion of the reaction, the mixture was evaporated under vacuum. The residue was dissolved in DCM (50 mL) and washed with water (50 mL). The organic phase was washed with brine and dried over Na₂SO₄ overnight. The solvent was evaporated under vacuum to give intermediate **27** (3.50 g, 92.1% yield). m.p.: 184–187 °C. ¹H NMR (300 MHz, CDCl₃) δ (ppm): 8.34 (1H, d, J = 7.6 Hz, ArH), 7.90 (1H, d, J = 6.9 Hz, ArH), 7.57 (1H, t, J = 53.6 Hz, CHF₂), 7.48–7.39 (2H, m, ArH), 3.92–3.85 (8H, m, CH₂), 3.80 (4H, s, CH₂), 3.55 (4H, s, CH₂), 1.50 (9H, s, CH₃).

To a solution of compound **27** (3.50 g, 6.78 mmol) in EtOAc (20 mL) was added the EtOAc solution of HCl (10 mL). The mixture was stirred at 25 °C for 5 h. The reaction was checked by TLC. After completion of the reaction, the precipitate was filtered and washed with EtOAc, then dried under vacuum to give intermediate **29** as white solid (2.72 g, 88.6% yield). m.p.: 230–232 °C. ¹H NMR (300 MHz, CDCl₃) δ (ppm): 8.36 (1H, d, J = 7.3 Hz, ArH), 7.91 (1H, d, J = 7.1 Hz, ArH), 7.59 (1H, t, J = 53.7 Hz, CHF₂), 7.49–7.39 (2H, m, ArH), 3.98–3.87 (8H, m, CH₂), 3.81 (4H, s, CH₂), 3.02 (4H, s, CH₂).

Intermediate **15** (180 mg, 0.88 mmol), **28** or **29** (0.88 mmol) and PyBOP (550 mg, 1.06 mmol) were dissolved in DMF (20 mL), followed by the addition of DIPEA (0.44 mL, 2.64 mmol). The mixture was stirred at 25 °C for 8–10 h. The reaction was checked by TLC. After completion of the reaction, the solution was poured into water (60 mL) and stirred for 5 min. The precipitate was filtered and washed with water, then dried under vacuum. The crude product was purified by silica gel column chromatography (DCM/MeOH = 100:1 to 60:1) to yield the target compounds **5** and **11**.

4.2.11. 2-(4-(6-(2-(difluoromethyl)-1H-benzo[d]imidazol-1-yl)-2-morpholinopyrimidin-4-yl)piperazine-1-carbonyl)benzofuran-7-carboxamide (**5**)

The product was off-white solid, 45.3% yield, m.p.: 126–128 °C. HPLC: 98.03%. ¹H NMR (300 MHz, DMSO-*d*₆) δ (ppm): 8.23 (1H, d, J = 8.1 Hz, ArH), 7.91 (1H, d, J = 7.8 Hz, ArH), 7.84–7.80 (2H, m, ArH), 7.75 (1H, s, 1/2CONH₂), 7.70 (1H, t, J = 52.7 Hz, CHF₂), 7.56 (1H, s, ArH), 7.49–7.36 (3H, m, ArH), 6.04 (1H, s, ArH), 3.96–3.64 (16H, m, 6CH₂N, 2CH₂O). ¹³C NMR (75 MHz, DMSO-*d*₆) δ (ppm): 229.5, 197.7,

165.0, 163.8, 163.3, 162.4, 158.7, 153.7, 150.9, 148.6, 141.2, 127.6, 126.6, 125.4, 123.8, 121.8, 120.5, 119.9, 114.9, 111.0, 108.6, 79.5, 65.7, 45.8, 44.5, 25.8. HRMS (ESI): m/z [M+H]⁺. Calcd for C₃₀H₂₈F₂N₈O₄: 603.2274; Found: 603.2278. IR (cm⁻¹): 3362.8, 3195.9, 2967.3, 2866.9, 1685.0, 1635.7, 1618.1, 1604.2, 1524.3, 1449.5, 1425.25, 1392.5, 1347.1, 1283.9, 1235.4, 1227.8, 1216.2, 1200.4, 1188.1, 1114.8, 1094.6, 1041.2, 1011.7, 1002.6, 959.9, 768.7, 747.8, 736.1, 585.2.

4.2.12. 2-(4-(4-(2-(difluoromethyl)-1H-benzo[d]imidazol-1-yl)-6-morpholino-1,3,5-triazin-2-yl)piperazine-1-carbonyl)benzofuran-7-carboxamide (**11**)

The product was white solid, 41.4% yield, m.p.: 189–191 °C. ¹H NMR (300 MHz, CDCl₃) δ (ppm): 8.33 (1H, d, J = 7.7 Hz, ArH), 8.22 (1H, d, J = 7.3 Hz, ArH), 7.92 (1H, d, J = 7.1 Hz, ArH), 7.86 (1H, d, J = 8.0 Hz, ArH), 7.56 (1H, t, J = 53.6 Hz, CHF₂), 7.45 (3H, m, ArH), 7.35 (1H, s, ArH), 7.22 (1H, s, 1/2CONH₂), 6.02 (1H, s, 1/2CONH₂), 4.03–3.81 (16H, m, 6CH₂N, 2CH₂O). ¹³C NMR (75 MHz, DMSO-*d*₆) δ (ppm): 165.0, 164.3, 161.2, 158.8, 150.9, 148.6, 145.8, 141.3, 132.8, 127.6, 126.6, 125.9, 125.4, 124.3, 123.6, 120.6, 119.9, 115.8, 111.0, 108.5, 87.0, 65.8, 45.9, 43.6, 43.0. HRMS (ESI): m/z [M+H]⁺. Calcd for C₂₉H₂₇F₂N₉O₄: 604.2227; Found: 604.2233. IR (cm⁻¹): 3453.1, 3169.5, 2958.1, 2861.4, 1675.3, 1638.9, 1578.0, 1516.6, 1446.19, 1413.8, 1369.2, 1308.5, 1271.3, 1249.3, 1228.9, 1210.8, 1148.25, 1108.8, 1048.8, 1003.2, 983.3, 961.4, 849.6, 804.1, 765.5, 554.3, 539.9, 513.9.

4.3. Biological activity assay

4.3.1. In vitro PARP and PI3K inhibition assay

PARP-1/2 and PI3K $\alpha/\beta/\gamma/\delta$ inhibition assays were carried out according to previously reported procedures [27]. The IC₅₀ values were calculated using nonlinear regression with normalized dose-response fit using Prism GraphPad software.

4.3.2. In vitro antiproliferative activity assay

MDA-MB-468 cells were maintained in RPMI1640 medium containing 10% (v/v) FBS at 37 °C in a 5% (v/v) CO₂ humidified incubator. Cell proliferation assay was determined by the Cell Titer-Glo cell viability assay. Briefly, cells were passaged the day before dosing into a 96-well plate, allowed to grow for 12 h, and then treated with different concentrations of compound for 7 days at 5% CO₂, 37 °C. After incubation, 100 μ L of Cell Titer-Glo reagent was added to the assay plate, which was then incubated at room temperature for 10 min to stabilize luminescence signal and read by Envision plate reader. The inhibition rate (%) = (1 - (RLU compound-RLU blank)/(RLU DMSO-RLU blank)) \times 100%. The IC₅₀ values were calculated using nonlinear regression with normalized dose-response fit using XLFit software.

4.3.3. Real-time PCR

The relative expression of BRCA1 or BRCA2 mRNA was detected using Real-time PCR. Briefly, total RNA was extracted from cultured cells with TRIzol reagent (Life Technologies) according to the manufacturers' instructions. Reverse transcription reactions were performed using PrimeScript™ RT reagent Kit with gDNA Eraser (Takara). For transcript quantification, SYBR Green based qPCR was performed with PrimeScript™ RT Master Mix (Takara) using Real Time PCR System (Stratagene Mx3000p). The human BRCA1 forward primer was 5'-GTCCATCTGTCTGGAGTTGA-3', the reverse primer was 5'-AAAGGACACTGTGAAGGCC-3'. The human BRCA2 forward primer was 5'-AAAGGACACTGTGAAGGCC-3', and the reverse primer was 5'-TTCTCTCTCTTCATTGCG-3'. GAPDH was used as an internal control. The results were represented as fold changes relative to the internal control.

4.3.4. *In vivo* antitumor activity study

Six-week-old male BALB/c nude mice were purchased from the Beijing Vital River Laboratory Animal Technology Co., Ltd. All animals were housed in a specific pathogen-free facility and used according to the animal-care regulations of Nanjing Biorn Life Science Co., Ltd (Nanjing, Jiangsu, China). Prior to implantation, MDA-MB-468 cells were harvested during exponential growth. 2×10^6 cells were inoculated subcutaneously on the right flank of each BALB/c nude mouse. Mice were randomly divided into four treatment groups and control group when tumor size reached an approximate volume of 100 mm^3 . Olaparib (50 mg/kg), BKM120 (27.5 mg/kg), Olaparib + BKM120 (50 mg/kg + 27.5 mg/kg), and **12** (50 mg/kg) were administered every 2 days for 34 days (6 mice per group) by intraperitoneal administration, equal volume of PBS (5% DMSO, v/v) was used as the negative control. Tumor size and body weight were measured every 2 days. Tumor volume (V) was calculated using equation $V = ab^2/2$, where a and b stand for the longest and shortest diameter measured by vernier caliper, respectively.

4.4. Molecular modeling

The X-ray crystal structures of PARP-1 (PDB ID: 5DS3) and PI3K α (PDB ID: 4JPS) were retrieved from the Protein Data Bank. Molecular docking of compound **3** was carried out using the docking module of the Schrodinger Maestro 2019. The three-dimensional structures of compound **3** was constructed using ChemBio 3D Ultra software, then it was energetically minimized by using MMFF94 with 5000 iterations and minimum RMS gradient 0.05. The protein was prepared by the Protein preparation wizard of Schrodinger Maestro 2019. The waters were eliminated from the protein and the polar hydrogen was added. Receptor grids were generated using Receptor Grid Generation. The generated binding site was just the active pocket of PARP-1 or PI3K α , including several key amino acid residues. Compound lonicerin was placed during the molecular docking procedure. Types of interactions of the docked protein with ligand were analyzed after the end of molecular docking. The image files were generated using pymol 2.4.

Declaration of competing interest

The authors declare that they have no known competing financial interests or personal relationships that could have appeared to influence the work reported in this paper.

Acknowledgment

This work was supported by the National Natural Science Foundation of China (Grant No. 81502928) and Six Talent Peaks Project in Jiangsu Province, China (2017, YY-059).

Appendix A. Supplementary data

Supplementary data to this article can be found online at <https://doi.org/10.1016/j.ejmech.2020.113054>.

References

- [1] A.C. Garrido-Castro, N.U. Lin, K. Polyak, Insights into molecular classifications of triple-negative breast cancer: improving patient selection for treatment, *Canc. Discov.* 9 (2019) 176–198.
- [2] K.-L. Lee, Y.-C. Kuo, Y.-S. Ho, Y.-H. Huang, Triple-negative breast cancer: current understanding and future therapeutic breakthrough targeting cancer stemness, *Cancers* 11 (2019) 1334–1370.
- [3] J.X. He, T.H. Peng, Y.B. Peng, L.L. Ai, Z.Y. Deng, X.Q. Wang, W.H. Tan, Molecularly engineering triptolide with aptamers for high specificity and cytotoxicity for triple-negative breast cancer, *J. Am. Chem. Soc.* 142 (2020) 2699–2703.
- [4] L. Zhang, L.L. Fu, S.Y. Zhang, J. Zhang, Y.Q. Zhao, Y.X. Zheng, G. He, S.Y. Yang,

- L. Ouyang, B. Liu, Discovery of a small molecule targeting ULK1- modulated cell death of triple negative breast cancer in vitro and in vivo, *Chem. Sci.* 8 (2017) 2687–2701.
- [5] G.J. Yang, W.H. Wang, S.W.F. Mok, C. Wu, B.Y.K. Law, X.M. Miao, K.J. Wu, H.J. Zhong, C.Y. Wong, V.K.W. Wong, D.L. Ma, C.H. Leung, Selective inhibition of lysine-specific demethylase 5A (KDM5A) Using a Rhodium (III) complex for triple-negative breast cancer therapy, *Angew. Chem. Int. Ed.* 57 (2018) 13091–13095.
- [6] W.D. Zhang, W.Y. Yu, G.P. Cai, J.W. Zhu, C. Zhang, S.S. Li, J.P. Guo, G.P. Yin, C. Chen, L.Y. Kong, A new synthetic derivative of cryptotanshinone KYZ3 as STAT3 inhibitor for triple-negative breast cancer therapy, *Cell Death Dis.* 9 (2018) 1098–1109.
- [7] W.X. Zhou, C. Chen, X.Q. Liu, Y. Li, Y.L. Lin, X.T. Wu, L.Y. Kong, J.G. Luo, Discovery and optimization of withangulatin A derivatives as novel glutaminase 1 inhibitors for the treatment of triple-negative breast cancer, *Eur. J. Med. Chem.* (2020) 112980.
- [8] N. Cancer Genome Atlas Research, Integrated genomic analyses of ovarian carcinoma, *Nature* 474 (2011) 609–615.
- [9] N. Cancer Genome Atlas, Comprehensive molecular portraits of human breast tumours, *Nature* 490 (2012) 61–70.
- [10] R. Scully, A. Xie, G. Nagaraju, Molecular functions of BRCA1 in the DNA damage response, *Canc. Biol. Ther.* 3 (2004) 521–527.
- [11] R. Scully, N. Puget, BRCA1 and BRCA2 in hereditary breast cancer, *Biochimie* 84 (2002) 95–102.
- [12] M. Rouleau, A. Patel, M.J. Hendzel, S.H. Kaufmann, G.G. Poirier, PARP inhibition: PARP1 and beyond, *Nat. Rev. Canc.* 10 (2010) 293–301.
- [13] H. Farmer, N. McCabe, C.J. Lord, A.N. Tutt, D.A. Johnson, T.B. Richardson, M. Santarosa, K.J. Dillon, I. Hickson, C. Knights, N.M. Martin, S.P. Jackson, G.C. Smith, A. Ashworth, Targeting the DNA repair defect in BRCA mutant cells as a therapeutic strategy, *Nature* 434 (2005) 917–921.
- [14] A. Ashworth, A synthetic lethal therapeutic approach: poly(ADP-ribose) polymerase inhibitors for the treatment of cancers deficient in DNA double-strand break repair, *J. Clin. Oncol.* 26 (2008) 3785–3790.
- [15] C.J. Lord, M.D. Garrett, A. Ashworth, Targeting the double-strand DNA break repair pathway as a therapeutic strategy, *Clin. Canc. Res.* 12 (2006) 4463–4468.
- [16] K.A. Menear, C. Adcock, R. Boulter, X.L. Cockcroft, L. Copsey, A. Cranston, K.J. Dillon, J. Drzewiecki, S. Garman, S. Gomez, H. Javaid, F. Kerrigan, C. Knights, A. Lau, V.M. Loh Jr., I.T. Matthews, S. Moore, M.J. O'Connor, G.C. Smith, N.M. Martin, 4-[3-(4-Cyclopropanecarbonylpiperazine-1-carbonyl)-4-fluorobenzyl]-2H-phthalazin-1-one: a novel bioavailable inhibitor of poly-(ADP-ribose) polymerase-1, *J. Med. Chem.* 51 (2008) 6581–6591.
- [17] A. Tutt, M. Robson, J.E. Garber, S.M. Domchek, M.W. Audeh, J.N. Weitzel, et al., Oral poly(ADP-ribose) polymerase inhibitor olaparib in patients with BRCA1 or BRCA2 mutations and advanced breast cancer: a proof-of-concept trial, *Lancet* 376 (2010) 235–244.
- [18] H.D. Thomas, C.R. Calabrese, M.A. Batey, S. Canan, Z. Hostomsky, S. Kyle, K.A. Maegley, D.R. Newell, D. Skalitzyk, L.Z. Wang, S.E. Webber, N.J. Curtin, Preclinical selection of a novel poly(ADP-ribose) polymerase inhibitor for clinical trial, *Mol. Canc. Therapeut.* 6 (2007) 945–956.
- [19] P. Jones, S. Altamura, J. Boueres, F. Ferrigno, M. Fonsi, C. Giomini, S. Lamartina, E. Monteagudo, J.M. Ontoria, M.V. Orsale, M.C. Palumbi, S. Pesci, G. Roscilli, R. Scarpelli, C. SchultzFademrecht, C. Toniatti, M. Rowley, Discovery of 2-[(4-(3S)-piperidin-3-yl)phenyl]-2H-indazole-7-carboxamide (MK-4827): a novel oral poly(ADP-ribose) polymerase (PARP) inhibitor efficacious in BRCA-1 and -2 mutant tumors, *J. Med. Chem.* 52 (2009) 7170–7185.
- [20] P. Jones, K. Wilcoxon, M. Rowley, C. Toniatti, Niraparib: a poly(ADP-ribose) polymerase (PARP) inhibitor for the treatment of tumors with defective homologous recombination, *J. Med. Chem.* 58 (2015) 3302–3314.
- [21] B. Wang, D. Chu, Y. Feng, Y. Shen, M. Aoyagi-Scharber, L.E. Post, Discovery and characterization of (8S, 9R)-5-fluoro-8-(4-fluorophenyl)-9-(1-methyl-1H-1, 2, 4-triazol-5-yl)-2, 7, 8, 9-tetrahydro-3H-pyrido [4, 3, 2-de] phthalazin-3-one (BMN 673, talazoparib), a novel, highly potent, and orally efficacious poly(ADP-ribose) polymerase-1/2 inhibitor as an anticancer agent, *J. Med. Chem.* 59 (2016) 335–357.
- [22] C.J. Lord, A. Ashworth, Mechanisms of resistance to therapies targeting BRCA-mutant cancers, *Nat. Med.* 19 (2013) 1381–1388.
- [23] C.J. Lord, A. Ashworth, PARP inhibitors: synthetic lethality in the clinic, *Science* 355 (2017) 1152–1158.
- [24] K.K. Wong, J.A. Engelman, L.C. Cantley, Targeting the PI3K signaling pathway in cancer, *Curr. Opin. Genet. Dev.* 20 (2010) 87–90.
- [25] A. Kumar, O. Fernandez-Capetillo, A.C. Carrera, Nuclear phosphoinositide 3-kinase beta controls double-strand break DNA repair, *Proc. Natl. Acad. Sci. U. S. A.* 107 (2011) 7491–7496.
- [26] Y.H. Ibrahim, C. Garcia-Garcia, V. Serra, L. He, K. Torres-Lockhart, A. Prat, P. Anton, P. Cozar, M. Guzmán, J. Grueso, O. Rodríguez, M.T. Calvo, C. Aura, O. Díez, I.T. Rubio, J. Pérez, J. Rodón, J. Cortés, L.W. Ellisen, M. Scaltriti, J. Baselga, PI3K inhibition impairs BRCA1/2 expression and sensitizes BRCA-proficient triple-negative breast cancer to PARP inhibition, *Canc. Discov.* 2 (2012) 1036–1047.
- [27] A. Juvekar, L.N. Burga, H. Hu, E.P. Lunsford, Y.H. Ibrahim, J. Balmaña, A. Rajendran, A. Papa, K. Spencer, C.A. Lyssiotis, C. Nardella, P.P. Pandolfi, J. Baselga, R. Scully, J.M. Asara, L.C. Cantley, G.M. Wulf, Combining a PI3K inhibitor with a PARP inhibitor provides an effective therapy for BRCA1-related breast cancer, *Canc. Discov.* 2 (2012) 1048–1063.

- [28] U.A. Matulonis, G.M. Wulf, W.T. Barry, M. Birrer, S.N. Westin, S. Farooq, K.M. Bell-McGuinn, E. Obermayer, C. Whalen, T. Spagnoletti, W. Luo, H. Liu, R.C. Hok, C. Aghajanian, D.B. Solit, G.B. Mills, B.S. Taylor, H. Won, M.F. Berger, S. Palakurthi, J. Liu, L.C. Cantley, E. Winer, Phase I dose escalation study of the PI3kinase pathway inhibitor BKM120 and the oral poly (ADP ribose) polymerase (PARP) inhibitor olaparib for the treatment of high grade serous ovarian and breast cancer, *Ann. Oncol.* 28 (2017) 512–518.
- [29] A. Anighoro, J. Bajorath, G. Rastelli, Polypharmacology: challenges and opportunities in drug discovery: miniperspective, *J. Med. Chem.* 57 (2014) 7874–7887.
- [30] R. Morphy, Z. Rankovic, Designed multiple ligands, an emerging drug discovery paradigm, *J. Med. Chem.* 48 (2005) 6523–6543.
- [31] N.M. O'Boyle, M.J. Meegan, Designed multiple ligands for cancer therapy, *Curr. Med. Chem.* 18 (2011) 4722–4737.
- [32] J. Wang, H. Li, G. He, Z. Chu, K. Peng, Y. Ge, Q. Zhu, Y. Xu, Discovery of novel dual poly(ADP-ribose)polymerase (PARP) and phosphoinositide 3-kinase (PI3K) inhibitors as a promising strategy for cancer therapy, *J. Med. Chem.* 63 (2020) 122–139.
- [33] J.M. Dawicki-McKenna, M.F. Langelier, J.E. DeNizio, A.A. Riccio, C.D. Cao, K.R. Karch, M. McCauley, J.D. Steffen, B.E. Black, J.M. Pascal, PARP-1 activation requires local unfolding of an autoinhibitory domain, *Mol. Cell.* 60 (2015) 755–768.
- [34] S.M. Maira, S. Pecchi, A. Huang, M. Burger, M. Knapp, D. Sterker, C. Schnell, D. Guthy, T. Nagel, M. Wiesmann, S. Brachmann, C. Fritsch, M. Dorsch, P. Chene, K. Shoemaker, A. De Pover, D. Menezes, G. Martiny-Baron, D. Fabbro, C.J. Wilson, R. Schlegel, F. Hofmann, C. Garcia-Echeverria, W.R. Sellers, C.F. Voliva, Identification and characterization of NVP-BKM120, an orally available pan-class I PI3-kinase inhibitor, *Mol. Canc. Therapeut.* 11 (2012) 317–328.